Automated Searching of Ground Points from Airborne Lidar Data Using a Climbing and Sliding Method

Yi-Chen Shao and Liang-Chien Chen

Abstract

The extraction of a digital elevation model (DEM) from airborne lidar point clouds is an important task in the field of geoinformatics. In this paper, we describe a new automated scheme that utilizes the so-called "climbing-and-sliding" method to search for ground points from lidar point clouds for DEM generation. The new method has the capability of performing a local search while preserving the merits of a global treatment. This is done by emulating the natural movements of climbing and sliding in order to search for ground points on a terrain surface model. To improve efficiency and accuracy, the scheme is implemented with a pseudo-grid data and includes a back selection step for densification. The test data include a dataset released from the ISPRS Working Group III/3 and one for a mountainous area located in southern Taiwan. The experimental results indicate that the proposed method is capable at producing a high fidelity terrain model.

Introduction

The airborne light detection and ranging (lidar) system, which integrates a Global Positioning System (GPS), an Inertial Navigation System (INS), and a Laser scanning system, is a powerful instrument for the direct acquisition of 3D points for terrain modeling. It can efficiently and accurately acquire a high density of points for bare earth, as well as for vegetated areas and artificial above-ground objects. Over the past few years, the generation of digital elevation models (DEMs) from lidar point clouds has become one of its most important applications in relation to surveying and mapping.

The data acquired by the airborne lidar system is presented as 3D point clouds. These include ground points for bare earth, as well as object points for vegetation and artificial man-made objects such as buildings, bridges, towers, and power lines. Thus, DEM generation requires the selection of ground points, or the elimination of object points from the lidar data. A number of filtering algorithms have been proposed for DEM generation, but some of these have been developed only for specific terrain types, such as in urban (Morgan and Tempfli, 2000; Shan and Sampath, 2005) or forested areas (Haugerud and Harding, 2001; Raber *et al*, 2003). Most algorithms are designed with the intent of being able to cope with varied terrain types, so they are usually able to perform well for landscapes of moderate complexity (Sithole and Vosselman, 2003). However, processing errors still exist, due to constraints of these mathematical models or the data structure, especially for locations where slope discontinuities exist. One example of this is for break lines, which represent the edges of ground surfaces, such as ridges, dikes, or cliffs (Sithole and Vosselman, 2004). In order to achieve computational efficiency and obtain accurate results regardless of the terrain, we propose utilizing a new slope-based method in an automated scheme that is aptly called the climbing-and-sliding (CAS) method to search for ground points in pseudo-grid data. With the algorithm, we can take into account upward and downward motions, that is emulating the natural climbing and sliding movements. The proposed method has the advantage of performing a local ground point search while still preserving the merits of a global treatment.

Review of Related Filtering Methods

Most filtering methods are based on the assumption that there will be an abrupt change in height between an object point and the neighboring ground point. Under this assumption, the filtering processes can be divided into three categories: point-to-point, points-to-points, and point-to-points (or point-to-surface) (Sithole and Vosselman, 2003).

The slope-based methods use point-to-point processing to perform a filtering action on a local area. Considering slopes on a gradient map, a special kernel function is used to improve the performance on sloped terrain (Vosselman, 2000; Vosselman and Maas, 2001; Sithole, 2001). A variant slope-based filter proposed by Roggero (2001) is modified using Vosselman's method. The method uses locally linear regression on interpolated grid data and factors in the weight from the height difference and distance in the local operator. Shan and Sampath (2005) focused on urban areas and searched for ground points based on the slope constraints along a scan line. However, the slope-based algorithms are difficult to delineate rugged terrain with low vegetation, as well as to reserve ground points located on break lines (Sithole and Vosselman, 2003). Sithole and Vosselman (2005) later proposed a scanline-based segmentation method with a weighting function and a classification procedure based on topological relationships to improve the results for break line locations.

Center for Space and Remote Sensing Research (CSRSR), National Central University, 300, Jhongda Rd., Jhongli, Taiwan (ycshao@csrsr.ncu.edu.tw).

Photogrammetric Engineering & Remote Sensing
Vol. 74, No. 5, May 2008, pp. 625–635.

0099-1112/08/7405–0625/$3.00/0

The typical points-to-points approaches that include the morphological filtering (Kilian *et al.*, 1996), the clustering technique (Brovelli *et al.*, 2002), and the block minimum (Wack and Wimmer, 2002) assume that object points are locally higher. The morphological approach is quite sensitive to the operator size. If the size is too small, large objects such as buildings will be retained. On the other hand, if the operator is too large, locally higher ground points, such as those located on ridges or hilltops may be removed (Kilian *et al.*, 1996). In some progressive morphological filters, various sizes are applied in order to optimize the procedure (Petzold *et al.*, 1999; Morgan and Tempfli, 2000; Zhang *et al.* 2003). Although they are efficient in relation to processing in the raster domain, the interpolation of grid data from point clouds decreases the accuracy.

The surface-based methods, which use the point-to-surface concept, are the classical parameterized surface fitting methods. Kraus and Pfeifer (1998) and Pfeifer *et al.* (2001) applied linear prediction with least squares and robust estimation to determine the optimal ground surface by reducing the weights of above-ground points and outliers. Krzysteck (2003) introduced a hierarchical finite element approach for surface fitting, which was based on a triangulated irregular network (TIN) model. Another surface-based filtering method, proposed by Elmqvist (2001), fitted a ground surface by employing an active shape model with the minimization of the internal energy. Since their assumptions are based on a continuous surface model, it is difficult to retain ground points located on break lines and produces rounding errors in the vicinity at these linear ground features.

In some surface-based methods, the TIN model is used to select ground points iteratively, these are more suitable for a discontinuous surface. Axelsson (2000) proposed a progressive method for the densification of ground points. Haugerud and Harding (2001) suggested removing of the spiking points from the TIN model. Sohn and Dowman (2002) proposed an upward and downward densification based on the minimum description length. The operation is similar to the Axelsson's. They assumed the ground surface to be locally flat; the operation sometimes causes the surface of mountainous or hilly areas to appear flat.

Generally, it is easy to remove the artificial objects that have small areas and a closed outline of slope discontinuity. It is also easy to remove vegetated points on condition of good lidar penetration. However, a ridge or hilltop that is locally higher than other portions of the ground surface may resemble an above-ground object and is difficult to retain, as it is regarded as an artificial object. Furthermore, ground break lines have slope discontinuities, such as ridges or step edges, could result in over-smoothing.

Concept Behind the CAS Method

The proposed CAS method is based on the point-to-point approach. With it, we are able to overcome the aforementioned disadvantages and to retain the terrain features of ridge, hilltop, and break line. Before explaining the concept on which the CAS method is based, some observations of terrain characteristics are made. In general, in a local area ground points are supposed to be lower than object points. Thus, the locally lowest point has the highest possibility of being on the ground. In addition, a lower neighbor in a limited area near a known ground point also has a high possibility of being a ground point. Objects above the ground, such as buildings, vegetation, cars, etc. are locally higher and may have a closed outline with abrupt changes in height or slope discontinuities. There are some ground points, located on locally high ground, such as hills and ridges, which do not have closed outlines of slope discontinuity. Although a terrace on a hill may have a closed outline, it is generally larger than most above-ground objects, and to some extent slope continuity is preserved. Slope discontinuities in the terrain, such as for break lines, present as linear features indicating ground surface edges. Although objects and break lines may divide the ground surface, the points in each respective ground surface area will still maintain slope continuity.

The original idea on which the CAS method is based comes from the observation of a natural phenomenon, i.e., flowing water. If water is poured continuously, from the locally highest ground, it will flow downwards to the lower ground until the entire ground surface is covered. Since lidar point clouds contain only height without structure or texture information, it is difficult to discriminate the locally highest ground points from object points. In addition, though the lidar point clouds include a high density of height information, they do not contain an infinite number of ground points with which to perfectly reconstruct terrain surface. To extrapolate this idea, we simulate a continuous climbing movement from the various locally lowest points to the locally highest ground. The climbing is followed by a sliding motion that will pass through all of the lower points. The climbing movement reaches the top edge of a break line along the side of a smaller slope, and the sliding movement flows down through the bottom edge of the break line. In this manner, the ground points located on the edge of the slope discontinuity can be retained. Those points that travel from one location to another during climbing or sliding are classified as ground points, even though they may follow a mostly irregular path. As the action suggests, we call this method the climbing-and-sliding (CAS) algorithm.

To emulate the climbing movement on continuous terrain, the CAS employs slope constraints. Three parameters are selected for the climbing operation, namely the general slope, slope increment, and maximum slope. The general slope and the maximum slope are designed to check the absolute slope of the terrain, while the slope increment checks the relativity. The general slope is used to judge the terrain continuity and prevents the climbing movement over objects. The slope increment can be regarded as the curvature, for climbing on continuous terrain to reach the locally highest ground, such as ridges or hilltops. The maximum slope prevents the climbing at objects, for which the slope differential along the profile satisfies the slope increment. The sliding procedure simulates the flowing of water from higher to lower ground. The lower neighbors surrounding the ground seed or identified ground point are regarded as ground points.

Figure 1 illustrates the CAS process starting from three locally lowest points, the ground seeds, i.e., S_A, S_B, and S_C. The general slope allows for climbing from the seeds S_A, S_B, and S_C to search the neighboring ground points, G_A, G_C, and G_E, respectively. The general slope threshold also stops the climbing at a large slope, such as from G_A to O_A, G_C to G_B, or S_B to G_D. In terms of the slope increment, the difference between the slopes from S_B to G_C and G_C to G_B must satisfy the increment threshold, so G_B is identified as a ground point. A maximum threshold is needed to stop G_B from reaching on object point O_B. Thus, though point G_D on a steep slope will be excluded by the general slope and maximum slope thresholds, a sliding from the identified ground point G_E can include it.

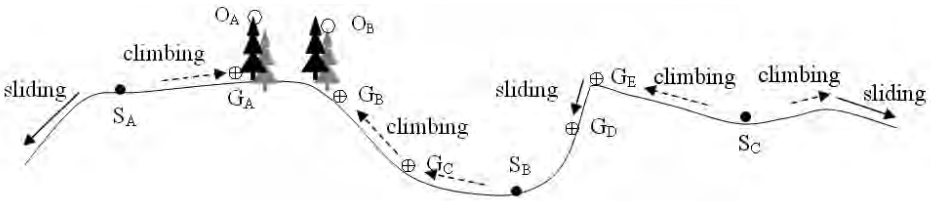

Figure 1. Illustration of the CAS process along a profile: •-Local lowest point as ground seed, ⊕-Searched ground point, ○-Object point.

The Proposed Scheme

To accelerate the process, we first reduce the original 3D point clouds into an initial surface model based on a pseudo-grid. To prevent noise from blocking the climbing and sliding movements, a preprocessing step is included to remove small objects and outliers. Subsequently, a region growing technique is applied to implement the CAS method of searching for ground points on the surface model. During the last step, a back selection process is used to select ground points that are omitted in the initial surface model. Figure 2 is a flowchart of the proposed scheme.

Generation of an Initial Surface Model

Significantly large amount of computation and memory is required to search for ground points from the original lidar 3D point clouds. To improve computational efficiency, piecewise or pyramid data can be used to determine the ground surface (Kraus and Pfeifer, 1998; Elmqvist, 2001). Some methods employ a coarse-to-fine approach (Axelsson, 2000; Sohn and Dowman, 2002; Wack and Wimmer, 2002). Since the DEM is a surface model, a grid data is favorable for computational efficiency. However, grid interpolation may decrease the accuracy of lidar data. Therefore, we employ a pseudo-grid selecting representative points for the initial surface model. Since the first step in our scheme is the initialization of the terrain model, some suitable representation points, although fewer in quantity, are justified. The lowest point in grid represents the grid elevation. In this way, most of the unwanted small object points will be excluded in the grid data. The original coordinates of these lowest points in grids are stored for further accurate computation. To retrieve some of the ground points are excluded at this stage, a back selection procedure is included. Despite the fact that the surface model is presented as a grid structure, no smoothing or interpolation is involved. The retained points represent the locally lowest elevation. Thus, the initial surface is a good approximation of the terrain surface. Figure 3 illustrates the pseudo-grid concept for the initial surface.

The CAS employs the concept of region growing in the pseudo-grids. Some grids could be empty due to an uneven distribution of the raw data. To avoid stopping the region growing, the empty grids are marked and filled with dummy values. The values are selected as the highest elevation of the surrounding area. Since an empty grid is filled with a higher value, it is unlikely to be regarded as a ground point. Even if some are classified as ground points in the subsequent process, the empty marker will prevent the inclusion of this point.

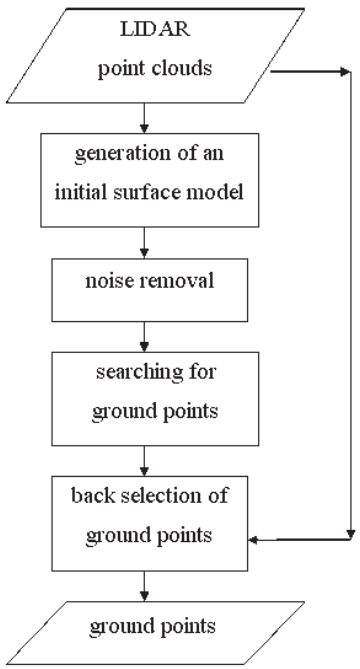

Figure 2. Flowchart of the process.

Noise Removal

A preprocessing is performed first to remove noise, such as outliers and low object points, on the initial surface. A flattening operation is used to replace the elevations of a noise area followed by a slope constraint to recover some ground points. These two processes of elevations replacement and point recovery are described as follows in detail.

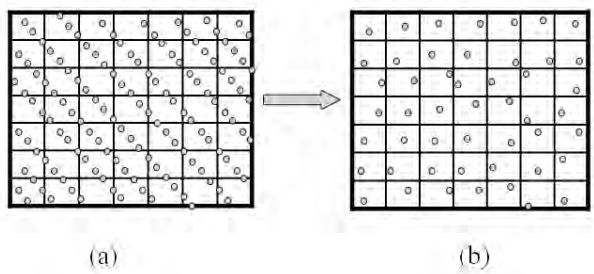

Figure 3. Pseudo-grid for surface initialization: (a) Original scanning points, and (b) Points on the initial surface model.

Object points above the ground and a few outliers could still exist in the initial surface model, and these should be removed. The implementation of the CAS process may be obstructed by some objects while searching for ground points. For instance, dense vegetation will block the climbing or sliding movement. Thus, to maximize the possible extension in the movement, we propose a preprocessing step to filter out the noise followed by searching for ground points. Here, we introduce two basic morphological operations, i.e., opening and closing with a flat structuring element (Dougherty, 1992) to remove noise on the initial surface. Opening includes erosion and dilation. Erosion is performed first to replace the center point by the lowest one in the operator; dilation selects the highest one. Opening removes locally higher points. On the other hand, closing first performs dilation followed by erosion. Closing removes locally lower points. A larger operator could result in over-smoothing, thus leading to information loss. Given that unwanted points are gathered in small areas, a 3×3 operator would be a good selection.

Some problems associated with the two morphological operations now need to be considered. Opening could remove some ground points located on the locally highest ground, such as ridges or hilltops. The slope constraint concept allows for the retention of these locally higher ground points. If the slope between the removed point and its un-removed ground neighbors satisfies the slope constraints, the removed point will be recovered. The closing operation could also eliminate some ground points in densely vegetated areas as low outliers. A wider grid of the surface model could exclude more vegetation points, so that ground points will not be so easily deemed low outliers. While processing a densely vegetated area, we suggest that opening is performed first to eliminate small object points and high outliers; subsequently followed by closing to remove low outliers.

Searching for Ground Points

In this step, the CAS process searches for ground points on the initial surface model. A region growing approach materializes the climbing and sliding movements starting from each ground seed. We can automatically search for the locally lowest point as seed in a selected square, for instance 80 m $\times$ 80 m. This avoids the seed being located on the top of a building. If there is a terrace on a hill with an area larger than the square, the generation of at least one seed is guaranteed. The processed points surrounding each ground seed are judged first by the CAS process. The identified ground points are then put into a queue for a first-in and first-out process. The CAS process searches for other ground points surrounding these identified points, and then extends to the global surface model.

The climbing process includes three parameters: the general slope $S_{general}$, the slope increment $dS_{increment}$, and the maximum slope S_{max}. The general slope considers only the relationship between two adjacent ground points. The slope increment is the slope differential along a profile and represents the second derivative of the height. It can be regarded as the curvature for climbing on continuous terrain to reach the locally highest ground. This extension operation is different from the traditional slope-based methods. The maximum slope prevents the inclusion of objects on gradually changing surfaces, such as for vegetation on sloped terrain. Since we employ the region growing technique, the window size is fixed at 3×3. Figure 4 shows the operating window, which is essentially a searching procedure, where a ground seed or an identified ground point P_0 and the processed surroundings P_1 to P_8 are to be classified. Although, this search may be simplified to a four-direction search, we prefer an eight-direction search, in order to reach an orientation-independent solution.

P_1	P_2	P_3
P_8	P_0	P_4
P_7	P_6	P_5

Figure 4. Operation window with a ground point P_0 and the processed surroundings P_1 to P_8.

If a processed point conforms to one of the two following conditions, it is classified as a ground point. The first condition can be described by Equation 1. If the slope S_{0i} from the ground point P_0 to a processed point P_i is less than the general threshold $S_{general}$, then P_i is classified as a ground point. Equation 2 delineates the second condition. Given two ground points P_0 and P_i and a processed point P_i, if the slope S_{0j} from P_0 to P_j is less than the maximum threshold S_{max}, and along a profile the slope difference dS_{ij} between S_{i0} and S_{0j} is less than the increment threshold $dS_{increment}$, then P_j is also classified as a ground point.

Given the characteristics of the sliding motion, when a processed point P_i is lower than the ground point P_0, then P_i is classified as a ground point. Since the slope S_{0i} from P_0 to P_i is negative and the general threshold $S_{general}$ is set to a positive value, the sliding process satisfies Equation 1, and no further calculation is needed.

$$\forall P_i \in G : S_{0i} \leq S_{general} \tag{1}$$

where P_0 is the identified ground point, P_i is the processed point, $i = 1 \sim 8$, G is the set of ground points, $S_{0i} = \dfrac{dH_{0i}}{D_{0i}}$ is the slope from P_0 to P_i, $dH_{0i} = H_i - H_0$ is the height difference from P_0 to P_i, $D_{0i} = \sqrt{(X_i - X_0)^2 + (Y_i - Y_0)^2}$ is the distance between P_0 and P_i, and $S_{general}$ is the threshold of the general slope parameter;

$$\forall P_j \in G : S_{0j} \leq S_{\max} \;\; and \;\; dS_{ij} \leq dS_{increment} \tag{2}$$

where P_i, P_0, P_j are the three points along a profile in the operation window, P_0, P_i are the identified ground points, $i = 1 \sim 8$, P_j is the processed points, $j = \begin{cases} i + 4, & i = 1 \sim 4 \\ i - 4, & i = 5 \sim 8 \end{cases}$, S_{i0}, S_{0j} are the slopes from P_i to P_0 and from P_0 to P_j, respectively, $dS_{ij} = S_{0j} - S_{i0}$ is the slope difference between S_{j0} and S_{i0}, S_{max} is the threshold of the maximum slope parameter, and $dS_{increment}$ is the threshold of the slope increment parameter.

Back Selection of Ground Points

The searched ground points with the above procedure can be used to generate an approximate DEM. However, in the initial surface model, made from lowest points in grids, other ground points in the same grids are neglected. Furthermore, some ground points in the surface model, such as in a courtyard or a vegetated area may not be successfully searched out by the CAS process, due to the blocking of the climbing and sliding movements. Thus, a secondary selection process for retrieving these missing ground points is necessary.

A general approach is to include more ground points so as to judge whether the normal distance from a potential point is close enough to the facet of the terrain TIN model

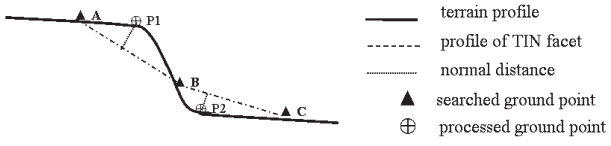

Figure 5. Profile illustration of points close to the break line with longer normal distances to the TIN facet.

(Axelsson, 2000). The selection of the normal distance threshold is sensitive to the places where ground points on a break might be excluded. In Figure 5, points A, B, and C are searched ground points from the previous procedures. Ground points P1 and P2, close to the break line, are missed in the initial surface and should be included during the back selection. To apply densification, by judging the normal distance to a TIN face, points P1 and P2 with longer distances could be neglected while using a smaller threshold. To accept this type of points by selecting a larger threshold, some lower objects on flat terrain could be misclassified as ground points. This is because the threshold of the normal distance is the function of (a) the sampling distance between identified ground points, (b) the slope of TIN facet, and (c) the slope of the terrain. By reapplying the sliding process, a processed point that is lower than the highest vertex of a facet is identified as a ground point. Since the outliers are removed from the initial surface, a point lower than the lowest vertex could be regarded as a low outlier and excluded. The back selection is made without needing another threshold and more points along the break line, such as step edge especially, will be retained. Based on experience, for most terrain types, a grid size of 4 to 6 m is appropriate to allow the initial surface. Since the searched points in the previous procedure are dense, one process is enough to select more ground points from the original data.

Experimental Test Data

Two data sets are included in the experiments to verify the proposed scheme. The first data set is released from the ISPRS Commission III, Working Group III and the second set is located in southern Taiwan. Given the variety of the ISPRS test data, the test results indicate that the proposed method is robust enough to model different landscape types and is insensitive to the operation parameters. To extend the test to denser vegetation and more complex terrain, a mountainous area in southern Taiwan is selected. Error computation for DEM generation is made, for the accuracy assessment, using on seven complex terrain samples with dense vegetation.

Test of the ISPRS Data

For the assessment of various terrain types, we employ data sets released from the ISPRS Working Group III/3 (ISPRS, 2004). The ISPRS test data were acquired by an Optech ALTM scanner over the Vaihingen/Enz test field and the Stuttgart city center. It includes eight sites comprised of different terrains: four urban areas and four rural areas with point spacing of 1 to 1.5 m and 2 to 3.5 m, respectively, as well as 15 reference samples of sub-areas. The terrain features of the 15 samples are described in Table 1.

We follow the quantitative assessment in ISPRS filter test (Sithole and Vosselman, 2003 and 2004) to validate the proposed scheme. Though our results consist of classified point lists, a TIN-based DEM generated from our searched ground points is easy for error computation. The ISPRS reference data that include ground and object points are compared to our DEM for error assessment. The errors and their magnitude and distribution are measured by using a height threshold of 20 cm, which is defined in the ISPRS filter test. Three kinds of errors are computed during the validation process, namely, type I errors, type II errors, and total errors. The type I error, i.e., omission error, would be where a reference ground point whose height difference compared to generated DEM is larger than 20 cm. The type II error, i.e., commission error, would be where a reference object point with height difference less than 20 cm. Figure 6 shows the definitions of these two types of errors. The total error is computed from the two types of errors. The

TABLE 1. FEATURES OF THE REFERENCE SAMPLES AT THE ISPRS FILTER TEST (SITHOLE AND VOSSELMAN, 2003)

Test Site	Reference Sample	Terrain Features	Range (m) ($dX \times dY \times dZ$)
Site1	Sample#1	vegetation and buildings on a steep slope	133.89 × 302.73 × 104.61
	Sample#2	small objects (cars)	204.38 × 264.22 × 21.53
Site2	Sample#3	narrow bridge	123.79 × 115.15 × 3.72
	Sample#4	buildings, crossover bridge and gangway	187.86 × 181.23 × 15.18
	Sample#5	complex buildings, large buildings, break lines	146.18 × 205.88 × 29.14
	Sample#6	ramp	121.86 × 72.44 × 20.85
Site3	Sample#7	courtyard	174.16 × 161.94 × 4.78
Site4	Sample#8	clump of low points	167.19 × 104.67 × 10.42
	Sample#9	railway station with trains	227.12 × 202.98 × 8.53
Site5	Sample#10	vegetation on slope	236.00 × 436.00 × 40.41
	Sample#11	low vegetation on sharp ridge	450.01 × 301.12 × 96.48
	Sample#12	break lines	432.00 × 476.00 × 79.05
	Sample#13	low resolution buildings	185.84 × 267.49 × 26.45
Site6	Sample#14	sharp ridge and ditches	508.00 × 448.00 × 37.91
Site7	Sample#15	land bridge	396.00 × 224.00 × 13.90

Filtered / Reference	ground	object
ground	a	b (type I error) (omission error)
object	c (type II error) (commission error)	d

Figure 6. Error definition.

percentage of type I, type II and total errors can be computed by Equations 3, 4, and 5, respectively.

$$\text{The percentage of type I error: } b/(a + b) \quad (3)$$

$$\text{The percentage of type II error: } c/(c + d) \quad (4)$$

$$\text{The percentage of total error: } (b + c)/(a + b + c + d) \quad (5)$$

where a, b, c, and d are defined as shown in Figure 6.

To test the sensitivity of the parameters selected for the proposed scheme, we use six sets of thresholds for error comparison. The selected thresholds include the grid size of the initial surface model and three slope parameters for the CAS process. The selected thresholds are shown in Table 2. Since we assume that unwanted points are gathered in small areas, the operating window for noise removal is set to 3×3. We employ the region growing technique to search for ground points; the window size is also fixed at 3×3. The error comparisons under different thresholds are shown in Figure 7.

TABLE 2. SIX SETS OF THRESHOLDS FOR ERROR COMPARISON

Parameter Set	Grid Size (m)	General Slope	Slope Increment	Maximum Slope
A	4	10%	5%	40%
B	4	10%	10%	40%
C	4	10%	10%	60%
D	6	10%	5%	40%
E	6	10%	10%	40%
F	6	10%	10%	60%

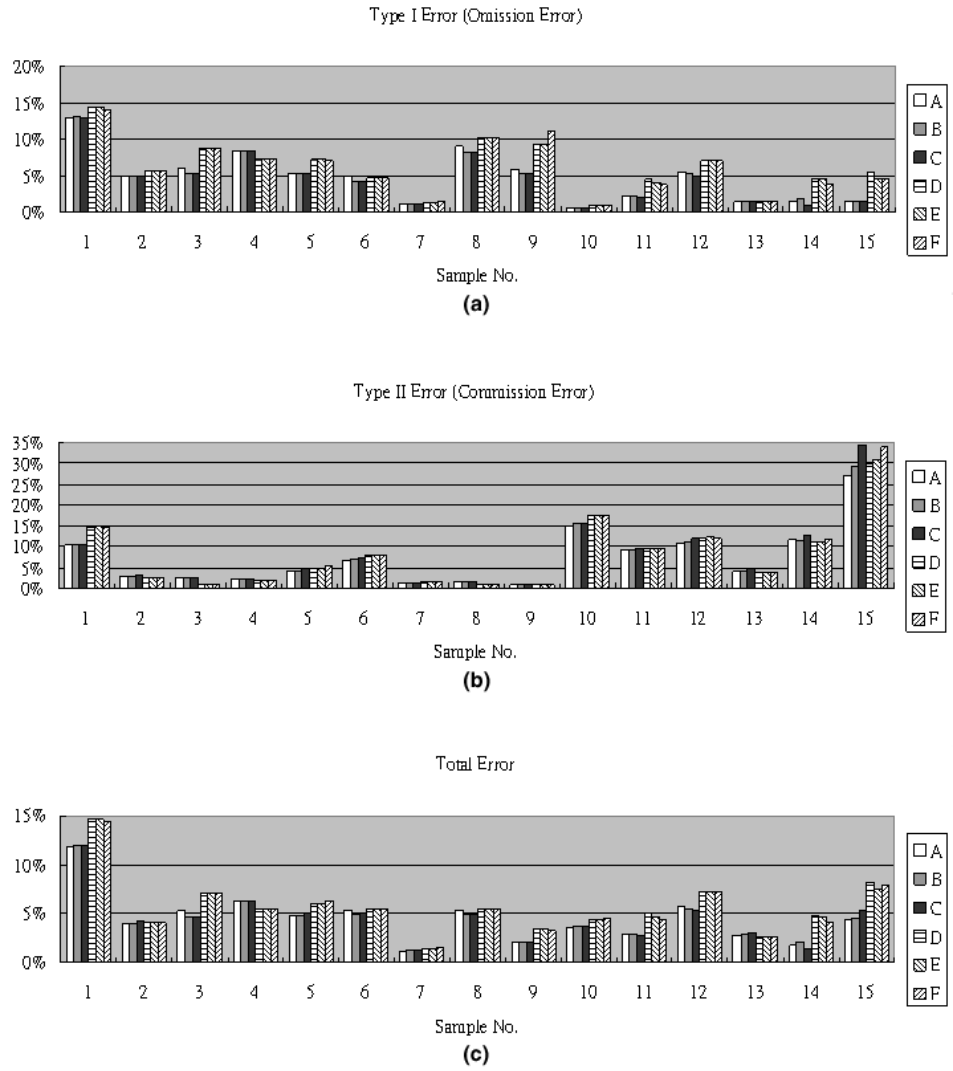

Figure 7. Error comparison with six threshold sets for the ISPRS reference samples: (a) Type I errors, (b) Type II errors, and (c) Total errors.

The total errors indicate that the slope parameters are insensitive to the results. Notice that the grid size would be more sensitive than the slope parameters. It can be seen that a 4 m grid is favorable for the test areas.

The results for total errors are also compared with three representative methods in the literature. The results are shown in Figure 8. The first one, i.e., Shao, is the result of the proposed method by employing the threshold set A in Table 2. The second one, suggested by Axelsson (2000), is based on the surface and region concept using progressive TIN densification for the selection of ground points. The third one, introduced by Kraus and Pfeifer (1998), relied on the surface concept. They used the classical least squares for the ground surface fitting. The last one is a modified slope-based method proposed by Roggero (2001). Although our thresholds are not optimized yet, the comparison indicates that the proposed method is superior to the other methods for samples 7, 8, 11, 12, 13, and 14. The remaining data sets are similar to the results of Axelsson (2000). Due to of the variety of the ISPRS test data, the results indicate that the proposed method is robust to different landscape types.

Visual inspection indicates that most of the terrain features are retained quite well. For instance, Figure 9 shows the processing result for reference sample 4, which contains buildings, a crossover bridge and a gangway in an urban site. Figure 9c shows the error map, giving the error definition in Figure 6. Moreover, Figure 10 shows the processing results for sample 12. Notice that the proposed method performs best for the areas with break lines. Figure 8 also indicates that we achieve the least total errors for the ridges, for instance, samples 11 and 14.

In samples 3, 4, 6, and 15 we can see a narrow bridge, a crossover bridge, a ramp and a land bridge, respectively. The bridge and ramp share similar geometric characteristics, as they both have two side break lines. Furthermore, the connection between two areas is essentially a small slope. The CAS method allows the ramp and land bridge, with their small slope over which the climbing movement can travel, are considered part of the ground. However, a crossover bridge with steep stairs may not be included, due to the general slope and the maximum slope constraints. Figure 9 shows that the crossover bridge in reference sample 4 has been removed. The land bridge in sample 15, which is shown in Figure 11, has been retained. Since the definition of a bridge in the ISPRS test is an attached object which rises vertically above the bare earth on only some sides, but not all, therefore, the type II error for reference sample 4 is low, but it is high for reference sample 15. However, a land bridge is easy to identify by visual inspection, so the points located on the bridge can easily be eliminated through manual editing.

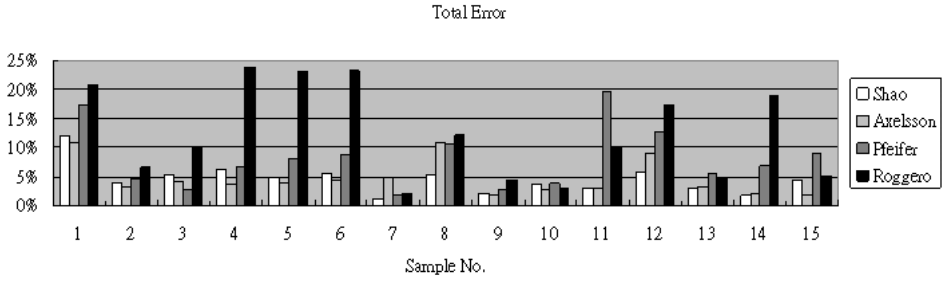

Figure 8. Total error comparison using the proposed method and three representations at the ISPRS filter test.

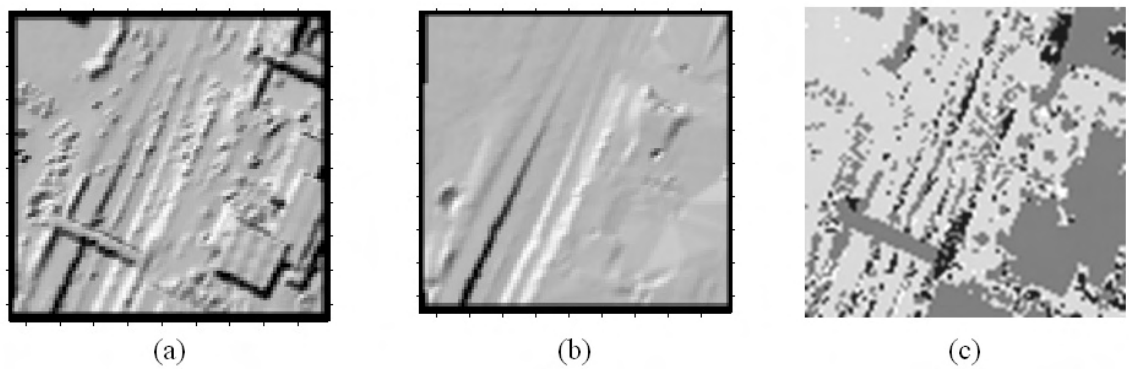

Figure 9. Shaded relief maps of sample 4 (buildings, crossover bridge and gangway): (a) Initial surface model, (b) Generated DEM excluding the crossover bridge, and (c) Error map (referring to Figure 6).

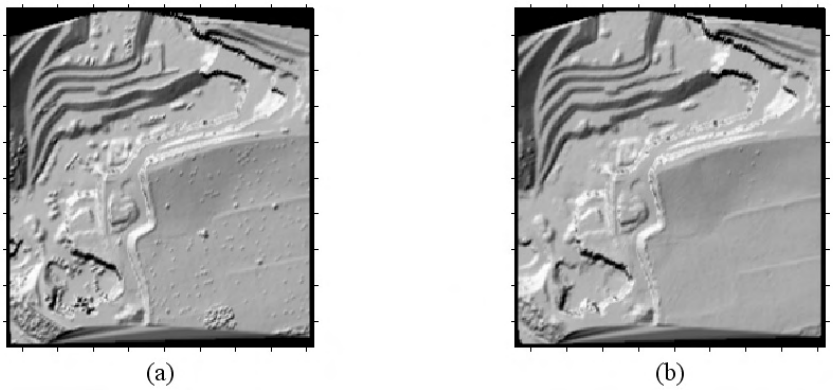

Figure 10. Shaded relief maps of sample 12 (break lines): (a) Initial surface model, and (b) Generated DEM.

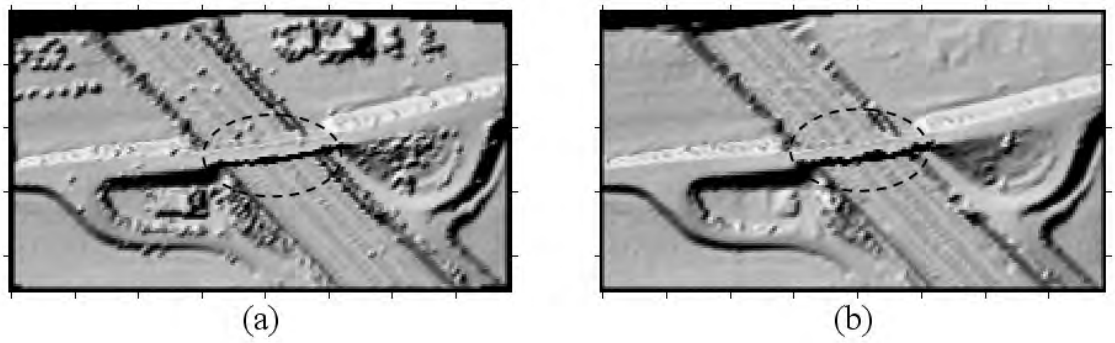

Figure 11. Shaded relief map of sample 15: (a) Initial surface model, and (b) Generated DEM including a land bridge.

In reference sample 1, which has vegetation and buildings on a steep slope, it is rather difficult to all the filtering algorithms, since the heights of the buildings and the vegetation are very close to the sloped ground. As a result many points may easily be misclassified, which could cause even greater total errors. For further assessment of this kind of terrain features by the proposed method, we employ a second data set, a mountainous area with dense vegetation. The results are discussed in the next section.

Test of a Mountainous Area

To extend the validation of the performance of the proposed method, a second data site was selected for mountainous area situated near Chishan town in southern Taiwan. The data was scanned by the Leica Geosystems ALS-50 system in October 2004. The flight speed was 120 knots and the height was 1,450 m, with a foot print of 0.3 m. The scanning frequency was 34 HZ and the pulse rate was 65.3 KHZ. The site covers an area of 1,350 m $\times$ 940 m with a point density of 1.8 pts/m^2. The ground elevation ranges from 59 m to 179 m. The terrain features in the test site are very diverse with an elevation range of 120 m in a small area, containing mountainous areas, vegetation, buildings, roads, rivers, bridges, and other artificial objects. Figure 12a shows an aerial image of the test site. Figures 12b and 12c show shaded relief maps of the initial surface model and generated DEM, respectively.

Seven representative areas are selected for testing. Squares A to G in Figure 12 depict the terrain characteristics. In Table 3, the terrain features are quantitatively described. To evaluate the accuracy of the generated DEM, a reference data set is generated by manual filtering and visual inspection of the aerial image. The computational error is based on grid data interpolated with a spacing of 2 m using the Kriging method. Table 3 also shows a summary of the accuracy assessment of the seven sample areas. Samples D and G, with dense vegetation on break lines, have larger errors than others.

A visual inspection confirms that the processing results represent the terrain features quite well. For instance, the river edge in sample B, the ridge and valley in sample C, and the break lines in sample G have all successfully been reconstructed. Samples D and G include a steep slope and tall trees with heights of 10 to 20 m, along with other vegetation located over the break lines. This complex type of terrain seems to produce larger errors. An inspection of a sample profile, as shown in Figure 13, shows that some ambiguities do exist. For example, it is hard to determine whether the solid line, the reference, or the dashed line, the filtered result, is correct. This ambiguity comes from having insufficient ground information, due to poor lidar penetration. However, the profile generated by the proposed scheme may be even more convincing than the manual one, thus, the accuracy in Table 3 could be underestimated.

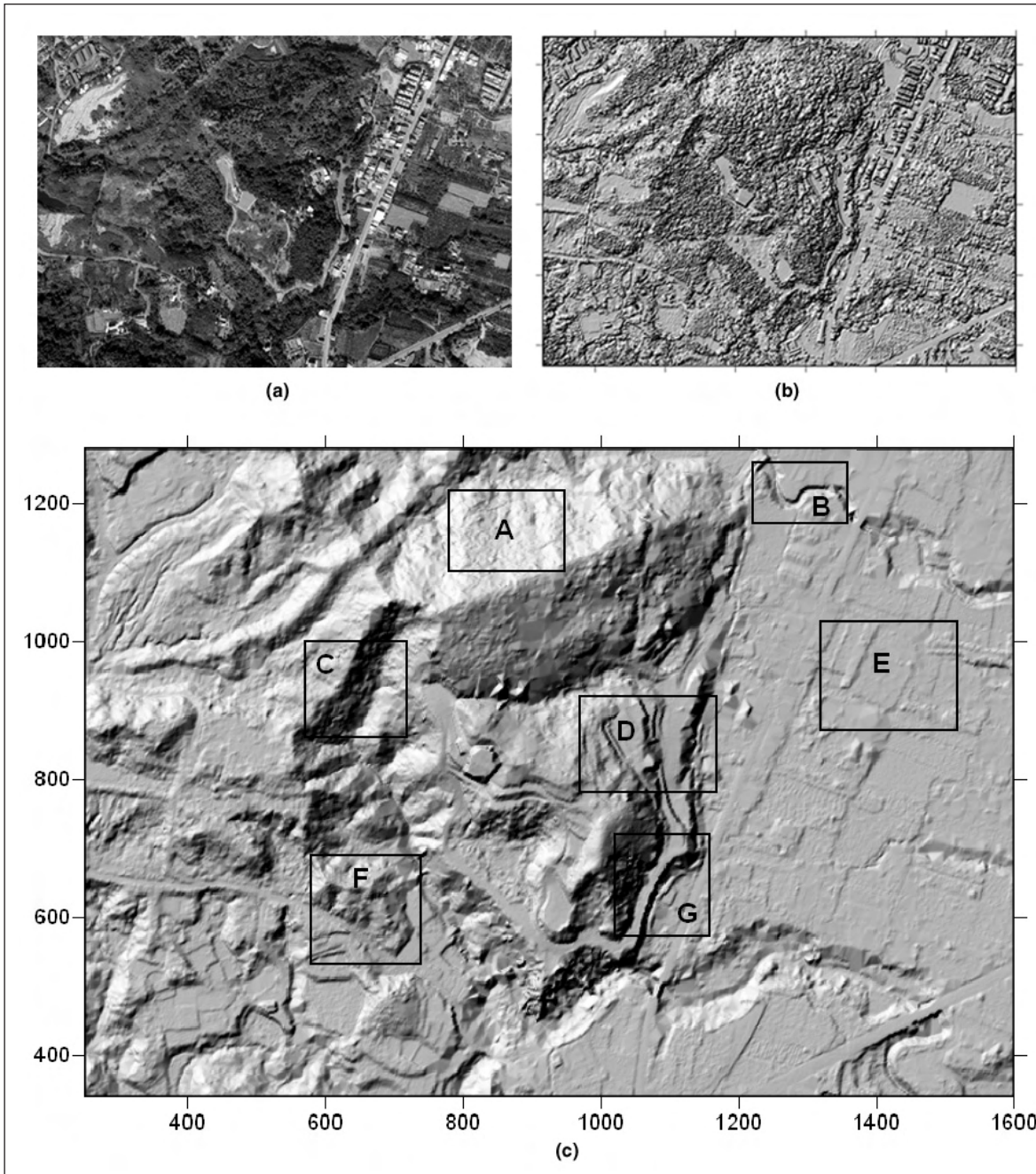

Figure 12. Test site in the mountainous area: (a) Aerial image, (b) Initial surface model, and (c) Generated DEM with seven reference samples (squares A to G).

Concluding Remarks

In this paper, we propose an automatic processing scheme for the searching of ground points from airborne lidar data. Based on the slope constraints, the CAS process searches for ground points by emulating the movements of both climbing and sliding over the surface model. A pseudo-grid data and a back selection of ground points are utilized for an efficient and accurate data processing.

Quantitative assessment of our results is carried out utilizing two data sets, an ISPRS filter test data and a mountainous area in southern Taiwan. The test with ISPRS data indicates that the slope parameters of the proposed scheme are insensitive to the results. On the other hand, the grid size of the initial surface model is more sensitive than the slope parameters. A comparison with three other representative methods at the ISPRS filter test shows that although our thresholds are not optimized, the proposed scheme presents favorable results in a number of terrain types. We observe that break lines in sample 12 and ridges in samples 11 and 14 are retained rather well and results in lower total errors. As well, although a land bridge in sample 15 is retained, it is easy to eliminate by manual editing through visual inspection.

The tests utilizing data from a mountainous area in Taiwan indicates that the terrain features and break lines, such as for ridges and valleys, are still retained. However, a steep densely vegetated slope may yield larger errors, due to the insufficiency of ground information from the poor lidar

TABLE 3. DEM ACCURACY ASSESSMENT FOR THE SEVEN SAMPLE AREAS. (UNITS: METERS)

Sample	Features	Area ($dX \times dY$)	Mean Error	RMSE	Min Error	Max Error
A	slope with dense vegetation	170 × 120	0.05	0.45	−2.45	4.46
B	narrow river	150 × 100	−0.10	0.43	−4.48	1.20
C	mountain ridge and valley	150 × 140	−0.04	0.46	−4.85	3.86
D	steep slope with buildings, vegetation and break lines	200 × 140	0.04	0.71	−4.14	10.55
E	plane with small buildings and low vegetation	200 × 160	−0.07	0.20	−1.79	0.83
F	small hill with dense vegetation	160 × 160	−0.08	0.54	−7.12	3.06
G	steep slope with vegetation and break lines	200 × 140	−0.08	0.72	−9.66	5.72

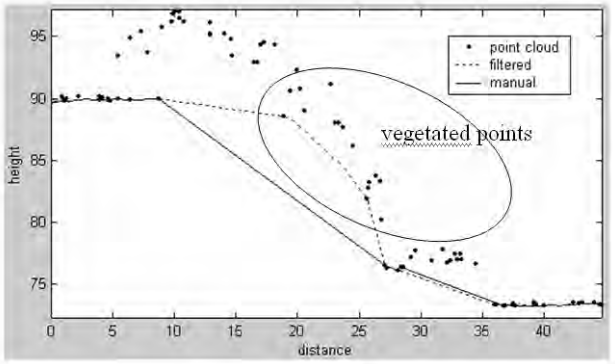

Figure 13. Profile ambiguity due to vegetation over the break line.

penetration. Further improvement is needed for such terrain, which could be a subject for future work.

Acknowledgments

The airborne lidar data in southern Taiwan was supported by the Department of Land Administration, M. O. I., and the Energy and Resources Laboratories of the Industrial Technology Research Institute. The stereo aerial images for object interpretation were supported by the Chinese Society of Photogrammetry and Remote Sensing.

References

Axelsson, P., 2000. DEM generation from laser scanner data using adaptive TIN models, *International Archives of the Photogrammetry, Remote Sensing and Spatial Information Sciences*, Vol. XXXIII (Pt. B4/1), pp.110–117.

Brovelli, M.A., M. Cannata, and U.M. Longoni, 2002. Managing and processing LIDAR data within GRASS, *Proceedings of the GRASS Users Conference*, Trento, Italy, 11–13 September, University of Trento, Italy, unpaginated CD-ROM.

Dougherty, E.R., 1992. *An Introduction to Morphological Image Processing*, SPIE Optical Engineering Press, Center for Imaging Science, Rochester Institute of Technology.

Elmqvist, M., 2001. Ground estimation of laser radar data using active shape models, *Proceedings of the OEEPE Workshop on Airborne Laserscanning and Interferometric SAR for Detailed Digital Elevation Models*, 01–03 March, OEEPE Publication No. 40, unpaginated CD-ROM.

Haugerud, R.A., and D.J. Harding, 2001. Some algorithms for virtual deforestation (VDF) of LIDAR topographic survey data, *International Archives of the Photogrammetry, Remote Sensing and Spatial Information Sciences*, XXXIV (Pt. 3/W4), pp. 211–218.

ISPRS, 2004. ISPRS test on extracting DEMs from point clouds: A comparison of existing automatic filters, ISPRS Commission III, Working Groups, URL: *http://www.geo.tudelft.nl/frs/isprs/filtertest/* (last date accessed: 25 January 2008).

Kilian, J., N. Haala, and M. Englich, 1996. Capture and evaluation of airborne laser scanner data, *International Archives of Photogrammetry and Remote Sensing*, Vienna, Austria, Vol. 31, Part B3, pp. 383–388.

Kraus, K., and N. Pfeifer, 1998. Determination of terrain models in wooded areas with airborne laser scanner data, *ISPRS Journal of Photogrammetry and Remote Sensing*, Vol. 53, pp. 193–203.

Krzystek, P., 2003. Filtering of laser scanning data in forest areas using finite elements, *Workshop Proceedings: 3-D Reconstruction from Airborne Laser Scanner and InSAR Data*, unpaginated CD–ROM.

Masaharua, H., and K. Ohtsuboa, 2002. A filtering method on airborne laser scanner data for complex terrain, *Proceedings of the ISPRS Commission III Symposium on Photogrammetric Computer Vision*, Graz, Austria, 09–13 September, unpaginated CD-ROM.

Morgan, M., and K. Tempfli, 2000. Automatic building extraction from airborne laser scanning data, *International Archives of Photogrammetry and Remote Sensing*, Vol. XXXIII, Part B3, pp. 616–622.

Petzold, B., P. Reiss, and W. Stössel, 1999. Laser scanning–Surveying and mapping agencies are using a new technique for the derivation of digital terrain models, *ISPRS Journal of Photogrammetry and Remote Sensing*, Vol. 54, pp. 95–104.

Pfeifer, N., P. Stadler, and C. Briese, 2001. Derivation of digital terrain models in the SCOP++ environment, *Proceedings of the OEEPE Workshop on Airborne Laserscanning and Interferometric SAR for Detailed Digital Elevation Models*, 01–03 March, Stockholm, Sweden, OEEPE Publication No. 40, unpaginated CD–ROM.

Raber, G.T., J.R. Jeansen, S.R. Schill, and K. Schuckman, 2002. Creation of digital terrain models using an adaptive lidar vegetation point removal process, *Photogrammetric Engineering & Remote Sensing*, 68(12):1307–1306.

Roggero, M., 2001. Airborne laser scanning: Clustering in raw data, *International Archives of the Photogrammetry, Remote Sensing and Spatial Information Sciences*, XXXIV (Pt. 3/W4), pp. 227–232.

Shan, J., and A. Sampath, 2005. Urban DEM generation from raw lidar data: A labeling algorithm and its performance, *Photogrammetric Engineering & Remote Sensing*, 71(2):217–226.

Sithole, G., 2001. Filtering of laser altimetry data using a slope adaptive filter, *International Archives of the Photogrammetry, Remote Sensing and Spatial Information Sciences*, XXXIV (Pt. 3/W4), pp. 203–210.

Sithole, G., and G. Vosselman, 2003. Comparison of filtering algorithms, *Proceedings of the Workshop* on 3-D Reconstruction from Airborne Laserscanner and InSAR Data, URL: *http://www.geo.tudelft.nl/frs/isprs/filtertest/* (last date accessed: 25 January 2008).

Sithole, G., and G. Vosselman, 2004. Experimental comparison of filter algorithms for bare-earth extraction from airborne laser scanning point clouds, *ISPRS Journal of Photogrammetry and Remote Sensing*, Vol. 59, pp. 85–101.

Sithole, G., and G. Vosselman, 2005. Filtering of airborne laser scanner data based on segmented point clouds, *Proceedings of the ISPRS WG III/3, III/4, V/3 Workshop: Laser Scanning 2005*, The Netherlands, 12–14 September, pp. 66–71.

Sohn, G., and I. Dowman, 2002. Terrain surface reconstruction by the use of tetrahedron model with the MDL Criterion, *International Archives of the Photogrammetry, Remote Sensing and Spatial Information Sciences*, XXXIV (Pt. 3A), pp. 336–344.

Vincent, L., and P. Soille, 1991. Watershed in digital spaces: An efficient algorithm based on immersion simulations, *IEEE Transactions on Pattern Analysis and Machine Intelligence*, 13(6):583–598.

Vosselman, G., 2000. Slope based filtering of laser altimetry data, *International Archives of the Photogrammetry, Remote Sensing and Spatial Information Sciences*, XXXIII (Pt. B3), pp. 935–942.

Vosselman, G., and H. Maas, 2001. Adjustment and filtering of raw laser altimetry data, *Proceedings of the OEEPE Workshop on Airborne Laserscanning and Interferometric SAR for Detailed Digital Elevation Models*, 01–03 March, Stockholm, Sweden, OEEPE Publication No. 40, unpaginated CD-ROM.

Wack, R., and A. Wimmer, 2002. Digital terrain models from airborne laser scanner data–A grid based approach, *International Archives of the Photogrammetry, Remote Sensing and Spatial Information Sciences*, XXXIV (Pt. 3B), pp. 293–296.

Zhang, K., and S.-C. Chen, 2003. A progressive morphological filter for removing non-ground measurements from airborne LIDAR data, *IEEE Transactions on Geoscience and Remote Sensing*, 41(4):871–882.

(Received 01 June 2006; accepted 18 September 2006; revised 01 November 2006)